Spectral analysis of Er^{3+}-, Er^{3+}/Yb^{3+}- and $Er^{3+}/Tm^{3+}/Yb^{3+}$-doped TeO_2–ZnO–WO_3–TiO_2–Na_2O glasses

2008 J. Phys.: Condens. Matter 20 375101

(http://iopscience.iop.org/0953-8984/20/37/375101)

J. Phys.: Condens. Matter **20** (2008) 375101 (8pp) doi:10.1088/0953-8984/20/37/375101

Spectral analysis of Er^{3+}-, Er^{3+}/Yb^{3+}- and $Er^{3+}/Tm^{3+}/Yb^{3+}$-doped TeO_2–ZnO–WO_3–TiO_2–Na_2O glasses

G Lakshminarayana[1,5], Jianrong Qiu[1], M G Brik[2], G A Kumar[3] and I V Kityk[4]

[1] State Key Laboratory of Silicon Materials, Zhejiang University, Hangzhou 310027, People's Republic of China
[2] Institute of Physics, University of Tartu, Riia 142, Tartu 51014, Estonia
[3] Department of Material Science and Engineering, The State University of New Jersey, NJ 08854-8065, USA
[4] Department of Chemistry, Silesian University of Technology, ulica Marcina Strzody 9, PL-44100 Gliwice, Poland

E-mail: glnphysics@rediffmail.com

Received 23 April 2008, in final form 28 May 2008
Published 12 August 2008
Online at stacks.iop.org/JPhysCM/20/375101

Abstract

In this paper, we present the spectroscopic properties of Er^{3+}-, Er^{3+}/Yb^{3+}- and $Er^{3+}/Tm^{3+}/Yb^{3+}$-doped novel tellurite glasses. From the measured absorption spectra, Judd–Ofelt (JO) intensity parameters (Ω_2, Ω_4 and Ω_6) have been evaluated for the Er^{3+}-doped glass. With 980 nm excitation three strong upconversion emission bands centered at 505, 520 and 630 nm were observed for both Er^{3+}- and Er^{3+}/Yb^{3+}-codoped glasses and the characteristic near-infrared emission bands were spectrally centered at 1.535 μm. The near-infrared spectra of Er^{3+}- and Er^{3+}/Yb^{3+}-doped glasses have shown full width at half-maxima (FWHM) around 100 nm and 120 nm for the erbium $^4I_{13/2} \rightarrow {}^4I_{15/2}$ transition, respectively. The measured maximum decay times of the $^4I_{13/2} \rightarrow {}^4I_{15/2}$ transition (at wavelength 1.535 μm) are about 7.24 ms and 7.68 ms for $1.0Er^{3+}$ and $1.0Er^{3+}/2Yb^{3+}$ (mol%)-codoped glasses, respectively. The maximum stimulated emission cross sections for the $^4I_{13/2} \rightarrow {}^4I_{15/2}$ transition of Er^{3+} and Er^{3+}/Yb^{3+} are 8.64×10^{-21} and 6.78×10^{-21} cm^2. From $1Er^{3+}/1Tm^{3+}/2Yb^{3+}$ (mol%)-codoped glass, broad near-infrared emission bands centered at 1510 nm (Er^{3+}:$^4I_{13/2} \rightarrow {}^4I_{15/2}$) and 1637 nm ($Tm^{3+}$:$^3F_4 \rightarrow {}^3H_6$) with full width at half-maxima (FWHM) around 52 nm and 60 nm, respectively, were observed. These glasses with broad near-infrared emissions should have potential applications in tunable lasers and broadband optical amplification at low-loss telecommunication windows

(Some figures in this article are in colour only in the electronic version)

1. Introduction

Recently, one can observe a renaissance in the study of rare-earth-doped materials for photonic applications, e.g. phosphors, display monitors, x-ray imaging, scintillators, lasers, upconversion and amplifiers for fiber-optic communications [1–9]. Rare-earth ions, especially erbium, have played an important role in the development of broadband erbium-doped fiber amplifiers (EDFA) in optical communication technology during the past few decades. It is known that erbium-doped glass has attracted much interest because of the $^4I_{13/2} \rightarrow {}^4I_{15/2}$ transition in Er^{3+} at a wavelength around 1.5 μm, coinciding with the low-loss transparent window of a standard optical communications fiber. For a practical standpoint, the flatness of the gain is also crucially important because the light

[5] Author to whom any correspondence should be addressed.

intensity for different channels would be varied by multistep amplifications. It is reported so far that the values of FWHM of 1.5 μm are 44, 65 and 85 nm for Al/P silica [10], fluozirconate [11, 12] and tellurite glass host [13], respectively. Yb^{3+} ions are used as sensitizers to enhance the pumping efficiency of 980 nm laser diode (LD) emission, since Yb^{3+} exhibits a large absorption cross section and a broad absorption band between 850 and 1080 nm compared with the weak absorption of Er^{3+} ions [14]. In this system, Yb^{3+} absorbs the radiation at 980 nm and transfers the energy to Er^{3+} (acceptor) according to the scheme $Yb^{3+}(^2F_{5/2}) + Er^{3+}(^4I_{15/2}) \rightarrow Yb^{3+}(^2F_{7/2}) + Er^{3+}(^4I_{11/2})$. The overall result is the increment of population in the level $^4I_{13/2}$ of Er^{3+}; as a consequence the luminescence intensity is stronger after relaxation to the ground state. It is well known that the dynamics of Er^{3+} emission depends on both Er^{3+} and Yb^{3+} concentrations and are strongly influenced by the optical properties of the host. Compared with silicate and borate glasses, tellurite glasses have more advantages as laser hosts due to their physical properties such as low melting temperature, high dielectric constant, high refractive index, large third-order nonlinear susceptibility and good infrared transmissivity. Furthermore, they present large transparency from the near-ultraviolet to the middle-infrared region. They are resistant to atmospheric moisture and capable of incorporating large concentrations of rare-earth ions into the matrix [15–25]. For the wavelength division multiplexing (WDM) system in the C-band, Er^{3+} in tellurites showed the highest emission cross section over the entire range of emission wavelengths. The optical, mechanical and chemical properties of the glass host depend on its composition. Therefore, the selection of the glass components is very important in the development of high performance tellurite glass. Recently, we have reported the NIR luminescence from Er^{3+}/Yb^{3+}, Tm^{3+}/Yb^{3+}, Er^{3+}/Tm^{3+} and Nd^{3+} ion-doped zincborotellurite glasses for optical amplification [26]. In those zincborotellurite glasses, the near-infrared spectra of Er^{3+}/Yb^{3+}-, Tm^{3+}/Yb^{3+}-, Er^{3+}/Tm^{3+}-and Nd^{3+}-doped glasses have shown full width at half-maxima (FWHM) around 58 nm (for $^4I_{13/2} \rightarrow {}^4I_{15/2}$ transition), 127 nm (for $^3F_4 \rightarrow {}^3H_6$ transition), 87 nm (for $^4I_{13/2} \rightarrow {}^4I_{15/2}$ transition) and 35 nm (for $^4F_{3/2} \rightarrow {}^4I_{11/2}$ transition), respectively. No studies have been found concerning the glass of the TeO_2–ZnO–WO_3–TiO_2–Na_2O system. The TeO_2 is the parent matrix; the ZnO is added in the parent matrix to cleave and/or elongate the Te–O bond in the basic TeO_4 trigonal bipyramid and facilitate easy glass formation [27]. Erbium-doped silicate and phosphate glasses compared to tellurite glasses have limited bandwidth for amplification and lower cross sections for the $^4I_{13/2}$ to $^4I_{15/2}$ transition. Because of the low phonon energy (<800 cm^{-1}) of the tellurite glass, the lifetime of the $^4I_{11/2}$ level of erbium ions is high compared to the lifetime of this level in phosphate and silicate glasses that have higher phonon energy. This in turn results in the low pumping efficiency under 980 nm excitation because of the occurrence of excited-state absorption(ESA) from this level to higher levels such as $^4F_{7/2}$ and low nonradiative decay rate to the lasing level $^4I_{13/2}$. Consequently, the gain in the $^4I_{13/2}$ to $^4I_{15/2}$ transition band of Er^{3+} will be affected. To overcome this deficiency usually tellurite glasses with higher phonon energy are made by adding tungsten and borate in tellurite glasses and increased phonon energies of 920 cm^{-1} and 1335 cm^{-1}, respectively, are reported [28]. So, in our studied tellurite glasses addition of tungsten is expected to decrease the lifetime of the $^4I_{11/2}$ level by multiphonon relaxation. Hence, an increase in the pumping efficiency at 980 nm, and amplifier gain for the $^4I_{13/2} \rightarrow {}^4I_{15/2}$ transition at 1.5 μm is possible. Addition of transition metal oxides to tellurite glasses is expected to increase the softening point and the glass stability, as demonstrated in the case of WO_3 [25]. Moreover, both WO_3 and TeO_2 components of the glass are network formers. As a result the glass contains two distinct types of dopant sites: those associated with WO_4 tetrahedral and WO_6 octahedral structural units and those associated with TeO_3 trigonal pyramid and TeO_4 trigonal bipyramid units [29]. The two types of dopant site have different geometries, and therefore different spatial distributions as well as the strength of ligand fields. As a consequence, the intensities of individual Stark transitions are different in the two types of site, giving rise to distinct spectral profiles. The resultant emission spectrum is then inhomogeneously broadened by combined contributions from all sites. The addition of TiO_2 produces a further increase of the linear and nonlinear refractive indices. The high linear index increases the local field correction at the rare-earth site leading to large radiative transition probabilities, whereas the nonlinear one enhances the optical nonlinearities [30–32]. Addition of Na_2O into glasses also provides suitability for the fabrication of optical waveguide devices by ion exchange. Also the addition of Na_2O improves the rare-earth solubility, leading to the possibility of using a high concentration of dopants, which is very important in the design of high efficiency short length fiber amplifiers.

In this paper, we have reported the results of NIR luminescence and upconversion properties of TeO_2–ZnO–WO_3–TiO_2–Na_2O, a new tellurite glass composition doped with Er^{3+} and Er^{3+}/Yb^{3+} ions. We have also prepared an $Er^{3+}/Tm^{3+}/Yb^{3+}$ ion-doped glass to study its near-infrared luminescence at both 1.5 μm (C-band) and 1.65 μm (U-band) wavelengths. It is well known that, in fiber-optics communication, C- and U-band wavelengths range from 1530–1565 nm and 1625–1675 nm, respectively [33].

2. Experimental studies

Following are the Er^{3+} and Er^{3+}/Yb^{3+} ion-doped tellurite glasses that have been developed for the present work, along with a reference glass:

$70TeO_2$–$10ZnO$–$10WO_3$–$5TiO_2$–$5Na_2O$(Host glass) (mol%)

$70TeO_2$–$10ZnO$–$10WO_3$–$5TiO_2$–$5Na_2O$–$1.0Er_2O_3$

$70TeO_2$–$10ZnO$–$10WO_3$–$5TiO_2$–$5Na_2O$–$1.0Er_2O_3/2Yb_2O_3$

$70TeO_2$–$10ZnO$–$10WO_3$–$5TiO_2$
–$5Na_2O$–$1.0Er_2O_3/1.0Tm_2O_3/2Yb_2O_3$.

The starting materials used in the present work were reagent grade of TeO_2, ZnO, WO_3, TiO_2, Na_2CO_3, Er_2O_3, Tm_2O_3 and Yb_2O_3. All weighed chemicals were powdered finely and mixed thoroughly before each batch (20 g) was melted at 930 °C for 30 min in a corundum crucible in air.

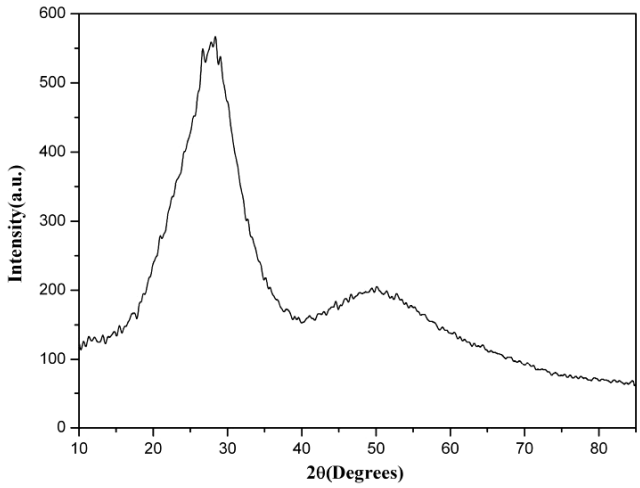

Figure 1. XRD spectrum of the $70TeO_2$–$10ZnO$–$10WO_3$–$5TiO_2$–$5Na_2O$ glass.

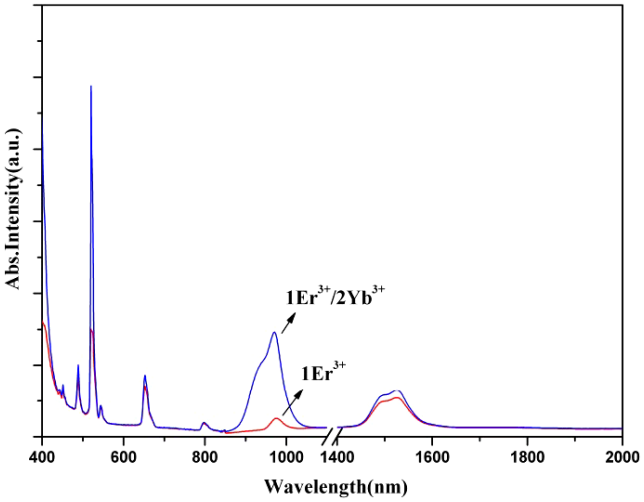

Figure 2. Absorption spectra of $1Er^{3+}$ and $1Er^{3+}/2Yb^{3+}$ (mol%) ion-doped glasses.

The melts were poured onto a preheated brass plate and then pressed by another plate. These glasses are in circular designs having 2–3 cm in diameter with a thickness of about 0.3 cm and with a good transparency. All the glasses were annealed at 300 °C for 10 h to remove thermal strains. Samples were cut and then polished to 2 mm thick slabs for different optical measurements.

The densities of the glasses were measured using the buoyancy method based on the Archimedes principle with toluene as an immersion liquid. An Abbe refractometer was used to measure the refractive indices at Na (589.3 nm) lamp wavelength. The powder x-ray diffraction (XRD) spectrum was obtained on a Rigaku D/MAX-RA diffractometer with an Ni filter and Cu Kα (=1.542 Å) radiation with an applied voltage of 340 kV and 20 mA anode current, calibrated with Si at the rate of 2 °C min^{-1}. The UV–vis/NIR absorption spectra were measured by a Hitachi F-4100 double-beam spectrophotometer with spectral resolution 1 cm^{-1}. The emission spectra were recorded by exciting the samples at 980 nm with an AlGaAs LD with cw power. The signal emitted was focused onto a SP-2357 monochromator (Acton Research) and detected by a thermoelectrically cooled InGaAs detector (Judson) and a photomultiplier tube R955 (Hamamatsu). We have also measured the NIR emission of an Er^{3+}/Yb^{3+}-codoped sample with 800 nm LD. The decay profiles corresponding to 1.53 μm were recorded using a SR540 chopper (Stanford Research System) at 15 Hz and connecting the photodetector directly to an oscilloscope (LT344 LeCroy). The overall response time of our detection system was <100 μs. The upconversion fluorescence spectra were recorded by a CCD-coupled spectrometer. All the optical measurements were performed at room temperature.

3. Results

Figure 1 presents the XRD pattern of the $70TeO_2$–$10ZnO$–$10WO_3$–$5TiO_2$–$5Na_2O$ glass, which confirms its amorphous structural nature. Figure 2 shows the absorption spectra of Er^{3+} and Er^{3+}/Yb^{3+} ion-doped glasses. From these spectra, absorption bands at 443 nm, 451 nm, 489 nm, 520 nm, 544 nm, 652 nm, 796 nm, 975 nm and 1525 nm which could be assigned to $^4F_{3/2}$, $^4F_{5/2}$, $^4F_{7/2}$, $^2H_{11/2}$, $^4S_{3/2}$, $^4F_{9/2}$, $^4I_{9/2}$, $^4I_{11/2}$ and $^4I_{13/2}$ from the ground state $^4I_{15/2}$,respectively, are well resolved. The experimental oscillator strengths (f) of the absorption spectral transitions of Er^{3+} doped in these glasses are calculated using the relation [34]

$$f_{\exp} = 4.318 \times 10^{-9} \int \varepsilon(\upsilon)\, \mathrm{d}\upsilon \tag{1}$$

where $\varepsilon(\upsilon)$ is the molar extinction coefficient at average energy (υ) in cm^{-1}. According to the f–f intensity model of JO theory [35, 36], the calculated oscillator strengths from the initial state to an excited state is given by

$$f\left(\Psi J; \Psi' J'\right) = \frac{8\pi^2 mc\upsilon}{3h\,(2J+1)} \left[\frac{\left(n^2+2\right)^2}{9n}\right] \times \sum_{\lambda=2,4,6} \Omega_\lambda \left(\Psi J \left\| U^\lambda \right\| \Psi'\, J'\right)^2 \tag{2}$$

where m is the mass of the electron, c is the velocity of light in vacuum, h is Planck's constant, n is the index of refraction of the glass, υ is the frequency of the transition $\Psi J \rightarrow \Psi^1 J^1$, $\Omega_\lambda (\lambda = 2,\ 4,\ 6)$ are the JO intensity parameters and $\|U^\lambda\|$ are the doubly reduced matrix elements of the unit tensor operator of the rank $\lambda = 2$, 4 and 6 which are calculated from the intermediate coupling approximation for a transition $\Psi J \rightarrow \Psi^1 J^1$. The experimental oscillator strengths of absorption bands of Er^{3+}-doped glass is determined with the known values of the Er^{3+} concentration, sample thickness, peak position and peak areas by using equation (1). We have applied least squares fitting procedure to determine the JO intensity parameters Ω_2, Ω_4 and Ω_6 by using the experimentally measured oscillator strengths and the obtained values are presented in table 1. The intensity parameters determined in the present investigation are found to be of the order $\Omega_2 > \Omega_4 > \Omega_6$, as shown in table 1. Generally,

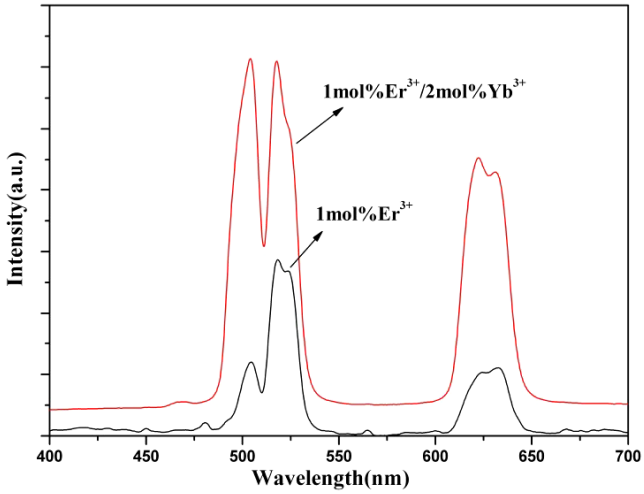

Figure 3. Upconversion emission spectra of $1Er^{3+}$ and $1Er^{3+}/2Yb^{3+}$ (mol%) ion-doped glasses.

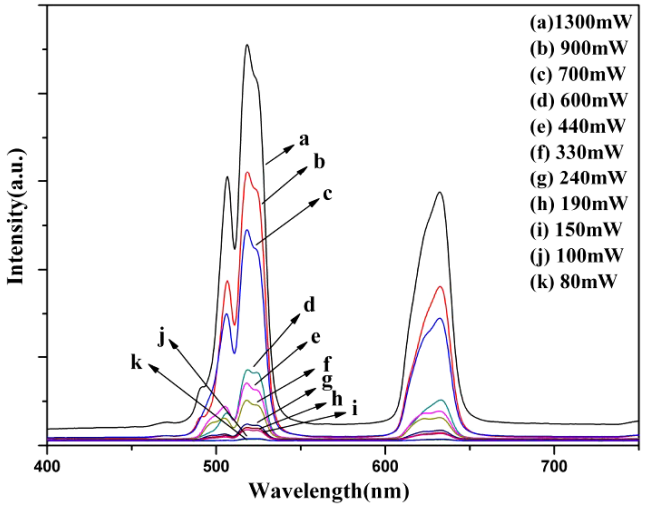

Figure 4. Upconversion emission spectra of $1Er^{3+}/2Yb^{3+}$ (mol%) ion-doped glass under different excitation power of 980 nm LD.

Table 1. Measured and calculated oscillator strengths ($f \times 10^{-6}$) and JO intensity parameters of 1.0 mol% Er^{3+} ion-doped glass. (Note: $\Omega_2 = 0.6592 \times 10^{-20}$ cm^2, $\Omega_4 = 0.3465 \times 10^{-20}$ cm^2, $\Omega_6 = 0.2575 \times 10^{-20}$ cm^2.)

Band	Energy (cm^{-1})	$\int \alpha d\lambda$ (10^{-7} cm)	f_{exp} (10^{-6})	f_{cal} (10^{-6})
$^4F_{5/2}$	22 148	0.6868	0.176 238	0.162 1039
$^4F_{7/2}$	20 449	2.189	0.478 865	0.549 63269
$^2H_{11/2}$	19 230	7.71	1.491 53	1.492 8772
$^4S_{3/2}$	18 382	0.9112	0.161 065	0.132 3303
$^4F_{9/2}$	15 325	5.178	0.636 188	0.627 3011
$^4I_{9/2}$	12 554	1.642	0.135 39	0.067 8637
$^4I_{11/2}$	10 272	3.608	0.199 15	0.156 856
$^4I_{13/2}$	6 548	17.93	0.402 242	0.350 8783

the Ω_2 parameter is sensitive to the symmetry of the rare-earth site and strongly affected by covalency between rare-earth ions and ligand anions, whereas Ω_4 and Ω_6 are related to the rigidity of the host medium in which the ions are situated. Figure 3 shows the upconversion spectra (excited at 980 nm) of the $1Er^{3+}$ and $1Er^{3+}/2Yb^{3+}$ (mol%)-codoped glasses. The observed emission bands could be assigned to $^2H_{11/2} \rightarrow {}^4I_{15/2}$ (505 nm), $^4S_{3/2} \rightarrow {}^4I_{15/2}$ (520 nm) and $^4F_{9/2} \rightarrow {}^4I_{15/2}$ (630 nm) transitions of Er^{3+} ions, respectively. The upconversion luminescence intensity in Er^{3+}/Yb^{3+}-codoped glass is much stronger than that of Er^{3+}-doped glass due to efficient energy transfer from Yb^{3+} to Er^{3+}. It is interesting to notice that both green emissions at 505 nm and at 520 nm are in equal intensity for Er^{3+}/Yb^{3+}-codoped glass. The upconversion luminescence of Er^{3+} ions was usually baffled by the multiphonon relaxation. The multiphonon relaxation probability depends primarily upon the energy gap between two successive levels and the phonon energy of the host [37]. The nonradiative decay of the excited electronic states of rare-earth ions in solids is dominated by the highest energy phonons. If these vibrations are characterized by frequencies that are too high, they can prove deleterious to the upconversion process as the ion relaxes via the emission of phonons rather than photons. The low phonon energy of the host glass matrices will cause small multiphonon relaxation probabilities. Therefore, the multiphonon relaxation rates are critical in determining the upconversion efficiency. The maximum phonon energy of tellurite glasses (<800 cm^{-1}) is low compared to all other oxide glasses such as silicate, borate and phosphate glasses [38–40]. So an intense upconversion luminescence can be obtained in tellurite glasses with Er^{3+} and Er^{3+}/Yb^{3+} ions. Figure 4 presents the upconversion emission spectra (excited at 980 nm) of Er^{3+}/Yb^{3+}-codoped glass under different excitation power. The green emission bands at 505 nm ($^2H_{11/2} \rightarrow {}^4I_{15/2}$) and 520 nm ($^4S_{3/2} \rightarrow {}^4I_{15/2}$) and red emission band at 630 nm ($^4F_{9/2} \rightarrow {}^4I_{15/2}$) are all considerably increased with an increment in excitation pump power. The integrated upconverted (I_{upc}) signal was plotted (not shown) as a function of the pumping power (I_{pp}). The experimental data were fitted by the expression $I_{upc} = kI_{pp}^n$, where n denotes the number of photons involved in the process and k is the proportionality constant. In our case, for green and red emissions, we found $n \sim 2$. Figure 5 presents the near-infrared emission spectra of Er^{3+}-and Er^{3+}/Yb^{3+}-codoped glasses. From these spectra, we have observed a broad emission band centered at 1535 nm ($^4I_{13/2} \rightarrow {}^4I_{15/2}$ transition), with full width at half-maximum (FWHM) around 100 nm for Er^{3+}-doped glass. For the Er^{3+}/Yb^{3+}-codoped glass, we have observed a broad emission centered at 1540 nm, with full width at half-maximum (FWHM) around 120 nm. We suggest that this broad 120 nm bandwidth is very useful for the EDFA at 1.5 μm wavelength. Because of the differences of the emission spectra of the different glass hosts, FWHM is often used as a semiquantitative indication of the bandwidth. The width of the emission band ($\Delta\lambda_{eff}$) for Er^{3+} ions at 1.5 μm is an important parameter for EDFA used in the WDM network system of optical communication. In order to satisfy the need of the increment of information capacity and improve the performance of the WDM network, a medium with a wide and flat gain at 1.5 μm, which is related to the width of the emission band, is required for the EDFA [41]. It

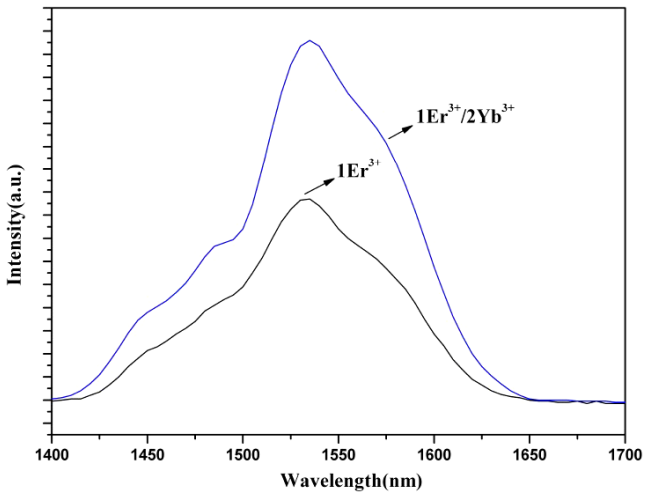

Figure 5. Near-infrared emission spectra of $1Er^{3+}$ and $1Er^{3+}/2Yb^{3+}$ (mol%) ion-doped glasses with 980 nm LD excitation.

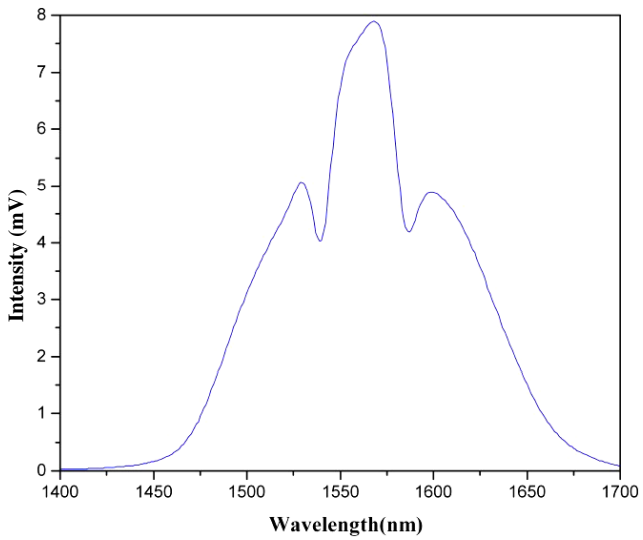

Figure 6. Near-infrared emission spectrum of $1Er^{3+}/2Yb^{3+}$ (mol%) ion-doped glass with 800 nm LD excitation.

is reported that the FWHM value of Er^{3+}-doped tungsten–tellurite glasses is 85 nm [42]. It is known that the main reason for the fluorescence broadening is the local crystal field symmetry at the rare-earth ion site. The inhomogeneous broadening is mainly due to the local structure and the coordination number of the Er^{3+} ions. It is also reported that WO_3 can form two different sites with $[WO_4]$ tetrahedral and $[WO_6]$ octahedral units and the structural units of TeO_2 glasses are TeO_4 trigonal bipyramids and TeO_3 trigonal pyramids [29, 43, 44]. Therefore, tungsten–tellurite glasses produce a complex network structure with greater variety of dopant sites of glass-forming constituents, WO_3 and TeO_2. In the studied glasses, the addition of a Ti^{4+} component could also help to modify the structure of the glass network and produces a complex network structure with a greater variety of dopant sites. Further work on structural investigations is definitely needed to explain the phenomenon. This result clearly suggests that the local crystal field generated in this new composition helps to broadband Er^{3+} emission at 1535 nm. Figure 6 presents the near-infrared emission spectrum of Er^{3+}/Yb^{3+}-codoped glass with 800 nm LD excitation. From this spectrum, we have observed the well-known NIR emission ($^4I_{13/2} \rightarrow {}^4I_{15/2}$) peak at 1567 nm with full width at half-maximum around 110 nm. It is interesting to notice that the emission peak changed from 1540 to 1567 nm, when the excitation wavelength changed from 980 to 800 nm (in both cases excitation power is 90 mW). Further studies are in progress to clarify this observed phenomenon. Figure 7 presents the near-infrared emission spectrum of $1Er^{3+}/1.0Tm^{3+}/2Yb^{3+}$ (mol%)-doped glass. From this spectrum both the near-infrared emissions of Er^{3+} and Tm^{3+} centered at 1510 nm ($^4I_{13/2} \rightarrow {}^4I_{15/2}$) and 1637 nm ($^3F_4 \rightarrow {}^3H_6$) [45] with full width at half-maximum(FWHM) around 52 and 60 nm were observed. The broad near-infrared emission band centered at 1637 nm, with FWHM around 60 nm that we observed in this $1Er^{3+}/1Tm^{3+}/2Yb^{3+}$ (mol%) glass, should have potential applications for U-band (1625–1675 nm) optical communication, including C-band (Er^{3+}:1510 nm emission).

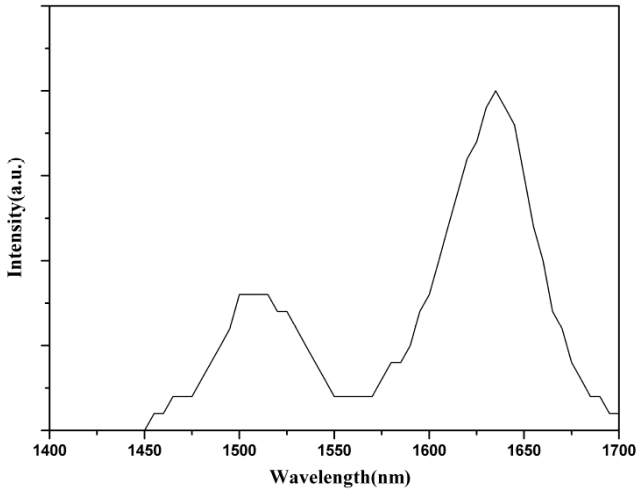

Figure 7. Near-infrared emission spectrum of $1Er^{3+}/1Tm^{3+}/2Yb^{3+}$ (mol%) ion-doped glass with 980 nm LD excitation.

Figures 8(a) and (b) show the luminescence decay curves of the $^4I_{13/2}$ state of Er^{3+} in Er^{3+}- and Er^{3+}/Yb^{3+}-codoped glasses by monitoring the $^4I_{13/2} \rightarrow {}^4I_{15/2}$ emission of Er^{3+}. In low Er-ion content glasses, there is a lower probability of nonradiative relaxation by ion–ion interaction. The fluorescence decay time of the $^4I_{13/2} \rightarrow {}^4I_{15/2}$ transition increases from 7.24 to 7.68 ms with an addition of 2 mol% Yb^{3+} ions.

4. Discussion

The increment in the fluorescence lifetime of the $^4I_{13/2}$ level is the result of the concentration optimization of the acceptor. The concentration effect is explained by differential site occupancy [42] and by the presence of the radiation trapping effect. In this phenomenon, photons spontaneously relaxed from the $^4I_{13/2}$ level are re-absorbed by the neighboring ions in the ground state ($^4I_{15/2}$). This process of re-absorption and re-

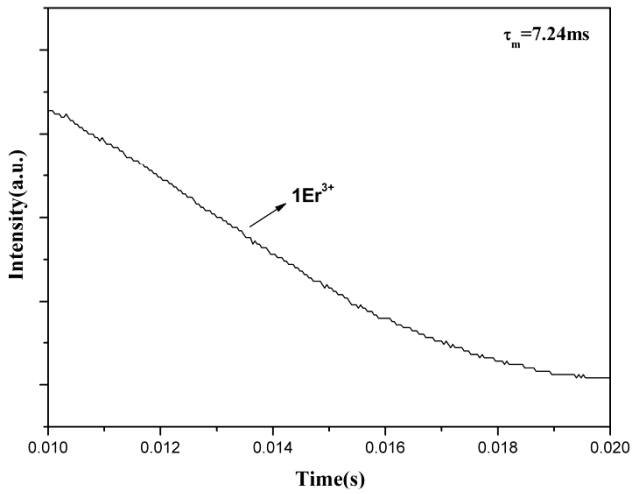

(a)

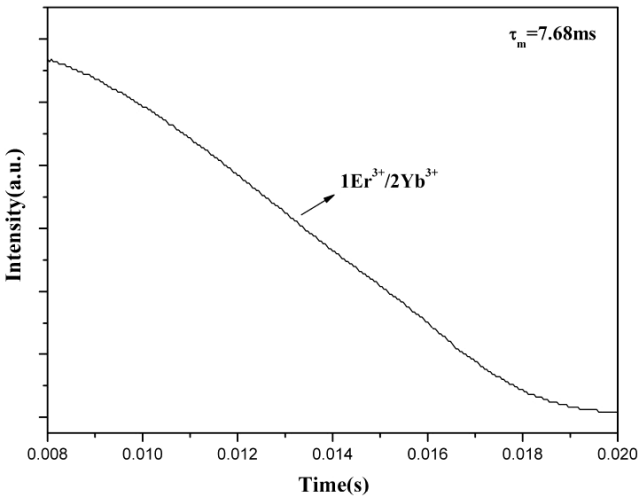

(b)

Figure 8. (a) Decay profile of $^4I_{13/2}$ of Er^{3+} emission in 1 mol% Er^{3+}-doped glass. (b) Decay profile of $^4I_{13/2}$ of Er^{3+} emission in $Er^{3+}/2Yb^{3+}$ (mol%)-codoped glass.

Table 2. Spectroscopic parameters of the 1.54 μm emission for Er^{3+} in the investigated Er^{3+} and Er^{3+}/Yb^{3+} glasses, fluorosilicate and ZBLAN hosts.

Hosts	$\sigma \times 10^{21}$ (cm^{-1})	τ (ms)	$\Delta\lambda_p$ (nm)	$\sigma\tau$	$\sigma\Delta\lambda$
Er^{3+} glass[a]	8.64	7.24	100	62.5	864
Er^{3+}/Yb^{3+} glass[a]	6.78	7.68	120	52	814
Fluorosilicate[b]	7.5	11.0	53	82.5	398
ZBLAN[b]	5.1	9.5	65	49	331

[a] In the present work.
[b] See [48].

emission is repeated and the overall result is an increase in the lifetime in comparison with a single isolated ion. The emission cross section is an important parameter and its value signifies the rate of energy extraction from the optical material. From the emission bands the stimulated emission cross section (σ_p^E)

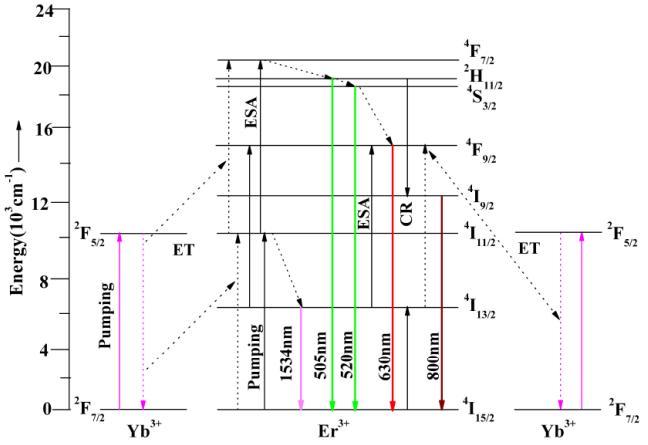

Figure 9. Energy diagram of the Er^{3+}/Yb^{3+} system and the mechanism proposed to explain both upconversion and infrared emissions.

could be estimated by

$$\sigma_p^E = \frac{\lambda_p^4}{8\prod cn_d^2\Delta\lambda_p\tau_m} \tag{3}$$

where c is the light velocity, n_d is the refractive index, λ_p is the emission peak wavelength, $\Delta\lambda_p$ is the width of the emission band which could be calculated by integrating the intensity of the luminescence lineshape and dividing it by the intensity at the peak wavelength and τ_m is the measured lifetime [46]. For an amplifier device, the figure of merit is defined as the product of lifetime and emission cross section, $\sigma\tau$. The gain bandwidth of an amplifier is determined largely by the width of the emission bandwidth and the value of the emission cross section, $\sigma\Delta\lambda_p$ [47]. The correlated spectroscopic parameters of the 1.54 μm emission for Er^{3+} in the investigated samples and other optical hosts are listed in table 2. It reveals that the presented Er^{3+} and Er^{3+}/Yb^{3+} glasses have superior near-infrared emission gain bandwidths compared to fluorosilicate and typical ZBLAN glasses. Figure 9 shows the energy level diagram of the Er^{3+}/Yb^{3+} system and the mechanism proposed to explain both upconversion and infrared emission. The predominant mechanisms of upconversion in these materials are excited state absorption (ESA) and energy transfer upconversion (ETU). According to this, the physical mechanism describing both visible and NIR emission is as follows. Er^{3+} ions (acceptors) are excited by the ET from Yb^{3+} (donor) that are excited directly ($^2F_{5/2} \rightarrow {}^2F_{7/2}$) by the pumping signal. In all cases the direct excitation of Er^{3+} is also possible; however, ET is most probably due to the larger absorption cross section of Yb^{3+} and the resonance between $^2F_{5/2} \rightarrow {}^2F_{7/2}$ and $^4I_{15/2} \rightarrow {}^4I_{11/2}$ transitions of Yb^{3+} and Er^{3+}, respectively, as shown in the energy diagram in figure 9. A part of the $^4I_{11/2}$ excited ions relaxes nonradiatively to the $^4I_{13/2}$ level and from there relaxes to the ground state, producing the 1.54 μm emission band. And another part was promoted to $^4F_{7/2}$ by the ET from the relaxation of another excited Yb^{3+} or Er^{3+} ($^4I_{11/2} \rightarrow {}^4I_{15/2}$) ion. The $^4F_{7/2}$ level decays nonradiatively to $^2H_{11/2} + {}^4S_{3/2}$

due to phonon energy. From there the population decays to the ground state producing the green emissions centered at 505 and 520 nm. Also a part decays nonradiatively to $^4F_{9/2}$ to finally decay to the ground state ($^4F_{9/2} \rightarrow {}^4I_{15/2}$) producing the red emission centered at 630 nm. So, for the red upconversion, the population of $^4F_{9/2}$ level is ascribed to the combined results of the ESA ($^4I_{13/2}$ + a photon $\rightarrow {}^4F_{9/2}$) CR between Er^{3+} ions: $^4I_{13/2} + {}^4I_{11/2} \rightarrow {}^4I_{15/2} + {}^4F_{9/2}$, ET from Yb^{3+} to Er^{3+} (Yb^{3+}:$^2F_{5/2}$ + Er^{3+} :^{4} $I_{13/2} \rightarrow Yb^{3+}$:$^2F_{7/2}$ + Er^{3+}:$^4F_{9/2}$), and a contribution of nonradiative relaxation from the higher energy level $^4S_{3/2}$ populated by means of the processes described previously. It is well known that the upconversion process is concentration-dependent. At higher concentrations, substantial energy transfer can occur between ions, since the energy transfer rate strongly depends on the distance between the ions. At low dopant concentration, ions are usually randomly distributed in the host and the $^4S_{3/2} \rightarrow {}^2H_{11/2}$ levels decay mostly radiatively to $^4I_{15/2}$. Therefore, the green emission has a higher intensity. The visible bands are also enhanced by increasing the excitation pump power. In this case, a part of the population in the $^4I_{13/2}$ level is promoted to $^4F_{9/2}$ by the ET from another donor $Yb^{3+}(^2F_{5/2}) + Er^{3+}(^4I_{13/2}) \rightarrow Yb^{3+}(^2F_{7/2}) + Er^{3+}(^4F_{9/2})$. It is also reported [49] that at a higher concentration ($>1.6 \times 10^{20}$ cm^{-3}), the luminescent lifetime of $^4S_{3/2}/^2H_{11/2}$ levels is shortened as a result of the cross-relaxation (CR) processes taking place between ($^2H_{11/2} \rightarrow {}^4I_{9/2}$) and ($^4I_{15/2} \rightarrow {}^4I_{13/2}$) transitions. The mechanism proposed for explaining the signals emitted by the codoped glass is well described in figure 9. Finally, it should be added that the rare-earth-doped tellurite glasses have demonstrated good nonlinear optical effects [50, 51], which opens the possibility for the fabrication of multi-functional quantum electronic devices.

5. Conclusions

In summary, we conclude that we have successfully prepared stable and moisture-resistant novel tellurite glasses with Er^{3+}, Er^{3+}/Yb^{3+} and $Er^{3+}/Tm^{3+}/Yb^{3+}$ as dopant ions, to study their optical properties. Strong green and red upconversion emissions were observed with 980 nm LD excitation in both Er^{3+} and Er^{3+}/Yb^{3+} ion-doped glasses. For Er^{3+}/Yb^{3+}-codoped glass, both green and red upconversion emission intensities were increased with an increment in excitation pump power at 980 nm. For Er^{3+}- and Er^{3+}/Yb^{3+}-codoped glasses, broad near-infrared emissions with FWHM around 100 nm and 120 nm centered at 1535 nm ($^4I_{13/2} \rightarrow {}^4I_{15/2}$) were obtained with 980 nm LD excitation. The maximum observed decay times of the $^4I_{13/2} \rightarrow {}^4I_{15/2}$ transition at wavelength 1535 nm are about 7.24 ms and 7.68 ms for Er^{3+}-and Er^{3+}/Yb^{3+}-codoped glasses, respectively. From the $Er^{3+}/Tm^{3+}/Yb^{3+}$-codoped glass, the observed near-infrared luminescence centered at 1510 nm (Er^{3+}:$^4I_{13/2} \rightarrow {}^4I_{15/2}$) and 1637 nm ($Tm^{3+}$:$^3F_4 \rightarrow {}^3H_6$) with FWHM values around 52 nm and 60 nm, respectively, could be so useful for the simultaneous optical amplification at both C- and U-bands. Therefore, tellurite–zinc–tungsten–titanium glasses are proposed to be good candidates for broadband EDFA. It can be concluded from our studies that Er^{3+}-, Er^{3+}/Yb^{3+}- and $Er^{3+}/Tm^{3+}/Yb^{3+}$-codoped TeO_2–ZnO–WO_3–TiO_2–Na_2O glasses are promising photonic materials for infrared amplifiers as well as the green and red upconversion emissions.

Acknowledgments

This work was financially supported by the National Nature Science Foundation of China (grant nos. 50672087 and 60778039), the National Basic Research Program of China (2006CB806007) and the National High Technology Program of China (2006AA03Z304). This work was also supported by the program for Changjiang Scholars and Innovative Research Team in University (IRT0651).

References

[1] Golding P S, Jackson S D, King T A and Pollnau M 2000 *Phys. Rev.* B **62** 856
[2] Pollnau M, Gamelin D R, Luthi S R, Gudel H U and Hehlen M P 2001 *Phys. Rev.* B **61** 3337
[3] Ferber S, Gaebler V and Eichler H J 2002 *Opt. Mater.* **20** 211
[4] Mortier M, Goldner P, Chateau C and Genotelle M 2001 *J. Alloys Compounds* **323/324** 245
[5] Qiao X S, Fan X P, Wang J and Wang M Q 2005 *J. Non-Cryst. Solids* **351** 357
[6] Vetrone F, Boyer J C, Capobianco J A, Speghini A and Bettinelli M 2002 *Appl. Phys. Lett.* **80** 1752
[7] Chung W J, Jha A, Shen S and Joshi P 2004 *Phil. Mag.* **84** 1197
[8] Kumar G A, De la Rosa E and Desirena H 2006 *Opt. Commun.* **260** 601
[9] Lin H, Jiang S, Wu J, Song F, Peyghambarian N and Pun E Y B 2003 *J. Phys. D: Appl. Phys.* **36** 812
[10] Miniscalco W J 1993 *Rare-Earth Doped Fiber Lasers and Amplifiers* ed M J F Diggonet (New York: Dekker)
[11] Miniscalco W J 1991 *J. Lightwave Technol.* **9** 234
[12] Semenkoff M, Guibert M, Ronarch D, Sorel Y and Kerdiles J F 1995 *J. Non-Cryst. Solids* **184** 240
[13] Mori A and Ohishi Y 1998 *Optical Fiber Communication Conf.* (*OSA Technical Digest Series* vol 6) (Washington, DC: Optical Society of America) WA1
[14] Hu Y, Jiang S, Sorbello G, Luo T, Ding Y, Hwang B C, Kim J H, Seo H J and Peyghambarian N 2001 *Proc. SPIE* **4282** 57
[15] El-Mallawany R 2002 *Tellurite Glasses Handbook, Physical Properties and Data* (Boca Raton, FL: CRC Press)
[16] Shen S, Naftaly M and Jha A 2002 *Opt. Commun.* **205** 101
[17] Shen S, Jha A, Lui X, Naftaly M, Bindra K, Bookey H and Kar A 2002 *J. Am. Ceram. Soc.* **85** 1391
[18] Chryssou C 2001 *Fiber Integr. Opt.* **20** 581
[19] Desirena H, De la Rosa E, Shulzgen A, Shabet S and Peyghambarian N 2008 *J. Phys. D: Appl. Phys.* **41** 095102
[20] Wang J S, Vogel E M and Snitzer E 1994 *Opt. Mater.* **3** 187
[21] Kim S H and Yoko T 1995 *J. Am. Ceram. Soc.* **78** 1061
[22] Özen G, Denis J-P, Genotelle M and Pellé F 1995 *J. Phys.: Condens. Matter* **7** 4325
[23] Sidebottom D L, Hruschka M A, Potter B G B and Brow R K 1997 *J. Non-Cryst. Solids* **222** 282
[24] Tanabe S, Hirao K and soga N 1990 *J. Non-Cryst. Solids* **122** 79
[25] Wang G, Xu S, Dai S, Zhang J and Jiang Z 2004 *J. Alloys Compounds* **373** 246
[26] Lakshminarayana G, Vidya Sagar R and Buddhudu S 2008 *J. Lumin.* **128** 690

[27] Burger H, Kneipp K, Hobert H, Vogel W, Kozhukarov V and Neov S 1992 *J. Non-Cryst. Solids* **151** 134
[28] Hocde S, Jiang S, Peng X, Peyghambarian N, Luo T and Morrell M 2004 *Opt. Mater.* **25** 149
[29] Himei Y, Osaka A, Namba T and Miura Y 1994 *J. Non-Cryst. Solids* **177** 164
[30] Kim S and Yoko T 1995 *J. Am. Ceram. Soc.* **78** 1061
[31] Lines M E 1991 *J. Appl. Phys.* **69** 6876
[32] Nasu H, Uchigaki T, Kamiya K, Kanbara H and Kubodera K 1992 *Japan. J. Appl. Phys.* **31** 3899
[33] Zhou S, Dong H, Zeng H, Wu B, Zhu B, Yang H, Xu S, Wan Z and Qiu J 2007 *J. Appl. Phys.* **102** 063106
[34] Lakshminarayana G and Buddhudu S 2006 *Phys.* B **373** 100
[35] Judd B R 1962 *Phys. Rev.* **127** 750
[36] Ofelt G S 1962 *J. Chem. Phys.* **37** 511
[37] Reisfeld R, Boehm L, Eckstein Y and Lieblich N 1975 *J. Lumin.* **10** 193
[38] Nandi P and Jose G 2006 *Opt. Commun.* **265** 588
[39] Jose R and Ohishi Y 2006 *Appl. Phys. Lett.* **89** 121122
[40] Joshi P, Shen S and Jha A 2008 *J. Appl. Phys.* **103** 083543
[41] Chen Y, Huang Y, Huang M L, Chen R P and Luo Z 2004 *Opt. Mater.* **25** 271
[42] Shen S, Naftaly M and Jha A 2002 *Opt. Commun.* **205** 101
[43] Himei Y, Osaka A, Nanba T and Miura Y 1994 *J. Non-Cryst. Solids* **177** 164
[44] Hager Z, El-Mallawany R and Poulain M 1999 *J. Mater. Sci.* **34** 5163
[45] Tikhomirov V K, Driesen K, Görller-Walrand C and Mortier M 2008 *Mater. Sci. Eng.* B **146** 66
[46] Karthikeyan B, Mohan S and Baesso M L 2003 *Physica* B **337** 249
[47] Shen S and Jha A 2004 *Opt. Mater.* **25** 321
[48] Jha M, Shen S and Naftaly M 2000 *Phys. Rev.* B **62** 6215
[49] El-Mallawany R, Patra A, Friend C S, Kapoor R and Prasad P S 2004 *Opt. Mater.* **26** 267
[50] Wasylak J, Ozga K, Kityk I V and Kucharski J 2004 *Infrared Phys. Technol.* **45** 253
[51] Wasylak J and Kityk I V 2007 *J. Eur. Ceram. Soc.* **27** 1703